JOURNAL OF COMPUTATIONAL PHYSICS 62, 124–142 (1986)

The Vector Potential in the Numerical Solution of Three-Dimensional Fluid Dynamics Problems in Multiply Connected Regions

A. K. WONG AND J. A. REIZES

School of Mechanical and Industrial Engineering, University of New South Wales, Kensington, N.S.W., Australia

Received March 21, 1984; revised January 8, 1985

The numerical solution of three-dimensional fluid flow problems in multiply connected regions using the vector potential formulation is reviewed. The major difficulty in such a formulation is the determination of boundary conditions for the vector potential. Two existing boundary formulations are examined, and it is shown that whilst one of the formulations leads to indeterminate vector potential boundary conditions for multiply connected solutions, the other presents well-defined conditions but is numerically not implementable. A new alternative is then proposed, and its validity and practicability are demonstrated with the solution of several annular cavity problems. © 1986 Academic Press, Inc.

1. INTRODUCTION

The idea of expressing a three-dimensional hydrodynamic velocity field in terms of a vector potential follows directly from Helmholtz's Decomposition Theorem (1858), which partly states that any vector field may be decomposed into curl-less and divergenceless components. In spite of such a longstanding recognition, the theory has to this date not been widely implemented in computations. The main reason for this has been the need for the solution of several additional variables, namely, the components of the vector potential and vorticity. Three-dimensional flow solvers are known to be computationally demanding, and the introduction of these variables inevitably further increases the computer memory requirement. However, in view that storage limitations will become less critical as modern computers become evermore powerful, and since Aziz and Hellums [1] have shown that the vector potential approach can lead to a faster and more stable convergence than that for the primitive variable formulation, the vector potential will undoubtedly play an increasingly important role in the solution of 3-D fluid dynamics problems. But for the present, the lack of research and development in the use of the vector potential has limited our understanding of this special variable. Although some workers have successfully applied the well-established formulation of Hirasaki and Hellums [2] to simply connected regions, and attempts have been made to use the relatively recent contribution of Richardson and Cornish [3] for multiply con-

0021-9991/86 $3.00

nected problems, few have understood the implications and consequences of these models.

It is the purpose of this paper to clarify and stress the limitations of the previously developed formulations, with special attention paid to multiply connected solutions. An alternate technique is then presented for dealing with the vector potential boundary conditions for some important multiply connected regions.

2. The Vector Potential Formulation

Use of the vector potential in solving the Navier–Stokes equations of fluid motion has been successful for flow problems in confined simply connected regions. Examples include the works of Aziz and Hellums [1], Mallinson and the Vahl Davis [4], and Ozoe et al. [5]. Any departure from the simplest form of solution regions, however, leads to much more complicated vector potential boundary conditions. Recently, Aregbesola and Burley [6] implemented the vector–scalar potential formulation of Hirasaki and Hellums [7] to tackle several through-flow problems. However, it has since been shown by Wong and Reizes [8] that the inclusion of the scalar potential destroys the most important feature of the vector potential (i.e., the automatic enforcement of local mass conservation) and can lead to significant errors in computations. An alternative formulation was presented in [8] to overcome the difficulty for at least an important class of through-flow problems, viz., flows in ducts of constant but arbitrary cross sections.

One area of the vector potential formulation which has remained unexplored is its application in multiply connected regions. This is largely due to uncertainty and confusion involved in determining the "correct" vector potential boundary conditions in such cases. Although Hirasaki and Hellums [2] presented a general boundary formulation which was thought to be applicable for multiply connected regions, it will be shown that their formulation is in fact incomplete. Richardson and Cornish [3] on the other hand had derived rigorously an alternate set of boundary conditions for a general region of any connectivity. However, the only reported implementation of this formulation by Leonardi et al. [9] had not been successful due to difficulties which will later become apparent.

Basic Equations

Since the derivation of the equations of motion in terms of the vorticity and vector potential may be found in many references (e.g., [4, 8]), the set of equations describing the motion of an incompressible fluid is therefore presented below without justification.

(a) *Vorticity Transport.*

$$\frac{\partial \boldsymbol{\zeta}}{\partial t} + (\mathbf{V}\cdot\nabla)\boldsymbol{\zeta} - (\boldsymbol{\zeta}\cdot\nabla)\mathbf{V} = \left(\frac{1}{Re}\right)\nabla^2\boldsymbol{\zeta} + \nabla\times\mathbf{F}, \tag{2.1}$$

where $\mathbf{V}$ is the velocity, *Re* is the Reynolds number, $\mathbf{F}$ is the body force, and ζ is the vorticity defined by

$$\zeta = \nabla \times \mathbf{V}. \tag{2.2}$$

(b) *Continuity*

$$\nabla \cdot \mathbf{V} = 0. \tag{2.3}$$

(c) *The Vector Potential.* The continuity equation is automatically satisfied if the velocity is expressed in terms of a vector potential ψ such that

$$\mathbf{V} = \nabla \times \psi. \tag{2.4}$$

The substitution of Eq. (2.4) into Eq. (2.2) yields, for a solenoidal vector potential field, the relationship

$$\nabla^2 \psi = -\zeta, \tag{2.5}$$

in which

$$\nabla \cdot \psi = 0. \tag{2.6}$$

The boundary conditions for the vorticity ζ are relatively straightforward, and various formulations have appeared in the literature (e.g., [4, 10]) which have been successfully implemented, and therefore warrant no further discussion.

The vector potential boundary conditions on the other hand require some attention as the non-uniqueness of the vector potential permits a multiplicity of its boundary formulation. In the derivation of Hirasaki and Hellums [2], only the normal component of velocity on the boundary is considered. This yields, for each of the distinct boundary surfaces, a second-order partial differential equation relating an auxiliary vector $\mathbf{B}$ (in which $\mathbf{B}$ is normal to the boundary surface, and whose surface-curl equals the tangential components of ψ), the geometric characteristics of the surface, and the normal component of the velocity on that surface. The above authors pointed out that for boundaries which coincide with one of the usually adopted coordinate surfaces (i.e., plane, cylindrical, and spherical surfaces), the boundary conditions for the vector potential reduce to relatively simple forms. For example, on a nonporous plane surface in Cartesian coordinates, whose normal is in the z-direction, the analysis can lead to the usually accepted conditions

$$\psi_x = \psi_y = \frac{\partial \psi_z}{\partial z} = 0. \tag{2.7}$$

Whilst the procedure of setting the boundary vector potential normal to the boundary surfaces is appropriate for a simply connected solution region, it is, however, not necessarily correct for the multiply connected case. Consider the doubly connected region shown in Fig. 2.1. On each of the solid surface, the more general

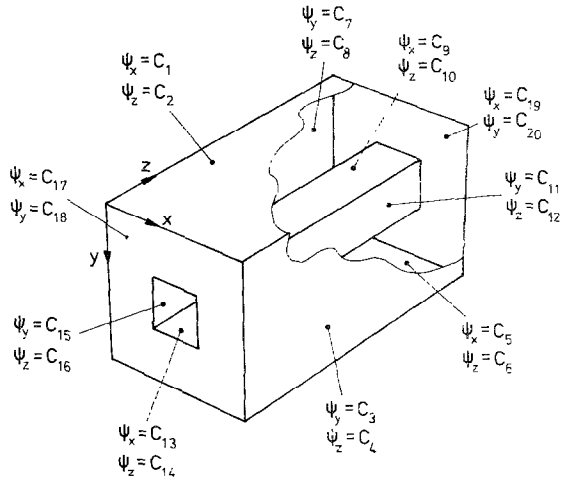

FIG. 2.1. Boundary conditions for the tangential components of ψ in a double connected region.

boundary formulation proposed by Hirasaki and Hellums [2] should apply. For instance, on the plane boundary whose normal is in the y-direction, we have

$$\frac{\partial \psi_x}{\partial y} = 0, \tag{2.8}$$

and

$$\frac{\partial^2 B_y}{\partial x^2} + \frac{\partial^2 B_y}{\partial z^2} = -V_y = 0, \tag{2.9}$$

where

$$\psi_x = \frac{-\partial B_y}{\partial z}, \qquad \psi_z = \frac{\partial B_y}{\partial x}. \tag{2.10}$$

One of the simplest non-trivial solutions of Eq. (2.9) is

$$B_y = \alpha x + \beta z + \gamma, \tag{2.11}$$

where α, β, and γ are constants. It then follows from Eq. (2.10) that

$$\psi_x = -\beta \qquad (= C_1, \text{ say}), \qquad \psi_z = \alpha = C_2. \tag{2.12}$$

Applying a similar analysis for the other boundaries gives the general result that the tangential components of the vector potential on each boundary may be set to a constant. For the solution region of Fig. 2.1, this results in 20 constants, C_1 to C_{20}, which are related by certain physical constraints. One necessary condition which

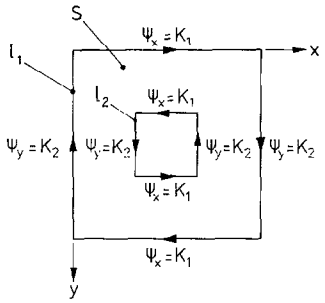

FIG. 2.2. $x - y$ cross section of the solution region.

was pointed out in [2] is that the vector potential must be continuous across the edge of any adjoining boundaries. This immediately requires that

$$\begin{aligned} C_1 = C_5 = C_9 = C_{13} = C_{17} = C_{19} \quad & (= K_1, \text{ say}), \\ C_3 = C_7 = C_{11} = C_{15} = C_{18} = C_{20} \quad & (= K_2), \\ C_2 = C_4 = C_6 = C_8 \quad & (= K_3), \\ C_{10} = C_{12} = C_{14} = C_{16} \quad & (= K_4). \end{aligned} \tag{2.13}$$

These four resulting constants (K_1 to K_4) are also not entirely arbitrary. As will be demonstrated, two of them (K_3 and K_4) are in fact related. Consider a cross section of the region parallel to the $x - y$ plane (Fig. 2.2). For steady incompressible flow, the net volumetric flow rate through this section must be zero. That is,

$$\iint_S \mathbf{V} \cdot \hat{\mathbf{n}}\, dS = 0, \tag{2.14}$$

or

$$\iint_S w\, dx\, dy = 0, \tag{2.15}$$

in which w is the z-component of V.

Writing w in terms of the vector potential, we have

$$\iint_S \left(\frac{\partial \psi_y}{\partial x} - \frac{\partial \psi_x}{\partial y} \right) dx\, dy = 0. \tag{2.16}$$

Applying Green's integral theorem for multiply connected plane surfaces, Eq. (2.16) becomes

$$\oint_{l_1} \psi_x\, dx + \oint_{l_1} \psi_y\, dy + \oint_{l_2} \psi_x\, dx + \oint_{l_2} \psi_y\, dy = 0, \tag{2.17}$$

where the sense of the above contour integrals is as indicated by the arrow heads in Fig. 2.2. It is easily seen from Fig. 2.2 that each of the integrals in Eq. (2.17) vanishes, so it follows that the condition described by Eq. (2.15) is satisfied, irrespective of the values of K_1 and K_2.

Consider now a cross-section parallel to the $x-z$ plane (Fig. 2.3). Again for steady-state conditions, the combined volumetric flow rate through the surfaces S_1 and S_2 is required to be zero. Application of Eq. (2.14) results in

$$\iint_{S_1} v\,dx\,dz + \iint_{S_2} v\,dx\,dz = 0, \tag{2.18}$$

which may be rewritten as

$$\iint_{S_1} v\,dx\,dz = -\iint_{S_2} v\,dx\,dz = Q \tag{2.19}$$

where v is the y-component of $\mathbf{V}$, and Q is the circumferential volumetric flow rate.

Expanding Eq. (2.19) and again applying Green's theorem results in

$$\oint_{l_3} \psi_x\,dx + \oint_{l_3} \psi_z\,dz = -\oint_{l_4} \psi_x\,dx - \oint_{l_4} \psi_z\,dz$$
$$= Q. \tag{2.20}$$

Performing each of the contour integrals yields

$$h(K_4 - K_3) = -h(K_3 - K_4). \tag{2.21}$$

Again, it is seen that the condition of zero net flow is satisfied irrespective of the values of K_3 and K_4. But since each side of Eq. (2.21) represents the circumferential volumetric flow rate Q, K_3 and K_4 cannot be chosen arbitrarily as Q must have some predetermined value which is dependent on the imposed physical conditions. The relationship between K_3 and K_4 may therefore be written as

$$K_4 = Q/h + K_3. \tag{2.22}$$

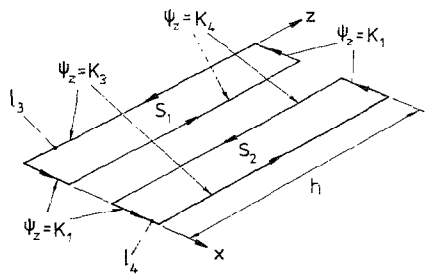

FIG. 2.3. $x-z$ cross section of the solution region.

With four constants and only one constraint (Eq. (2.22)), it is now apparent that three of the constants may be chosen arbitrarily. For simplicity, the value zero is the chosen, yielding

$$\begin{aligned} K_1 = K_2 = K_3 = 0, \\ K_4 = Q/h = K, \qquad \text{say.} \end{aligned} \tag{2.23}$$

Unfortunately, Eqs. (2.23) are yet of little use since in most cases Q is an unknown, and so it seems that an alternative formulation is required.

Richardson and Cornish [3] proposed a formulation which, at least in principle, may be used in multiply connected regions. Its development is complex, and the interested reader is referred to their paper for the full derivation. In contrast to the Hirasaki and Hellums formulation, they showed that it is possible to specify a vector potential whose normal component vanishes on the boundaries. That is,

$$\psi_n = 0 \tag{2.24}$$

on the boundaries.

The boundary conditions of the other components of ψ are then obtained by considering the tangential components of velocity on the surface. It may be shown that if Eq. (2.24) is satisfied on a boundary, then the definition of the vector potential (Eq. (2.4)) requires that

$$\begin{aligned} \frac{1}{\xi_{t_1}\xi_n}\frac{\partial}{\partial n}(\xi_{t_1}\psi_{t_1}) = V_{t_2}, \\ \frac{1}{\xi_{t_2}\xi_n}\frac{\partial}{\partial n}(\xi_{t_2}\psi_{t_2}) = -V_{t_1}, \end{aligned} \tag{2.25}$$

where ξ_n, ξ_{t_1}, ξ_{t_2} are scale factors, and n, t_1, t_2 denote the normal and the two independent tangential directions of the boundary surface, respectively.

For computational purposes, Eqs. (2.24) and (2.25) constitute a usable set of boundary conditions for the vector potential. However, its implementation by Leonardi et al. [9] yielded results which were later realised to be incorrect [11]. The problem stems from the fact that the normal velocity at the boundary is not forced to be zero, thereby permitting possible "leakages." Consider the solid boundary of a rectangular solution region which is contained in the $y-z$ plane. From Eqs. (2.24) and (2.25), the appropriate boundary conditions are

$$\begin{aligned} \psi_x = 0, \\ \frac{\partial \psi_y}{\partial x} = \frac{\partial \psi_z}{\partial x} = 0. \end{aligned} \tag{2.26}$$

For there to be no through-flow on this plane, the correct solution also requires

$$u = \frac{\partial \psi_z}{\partial y} - \frac{\partial \psi_y}{\partial z} = 0, \tag{2.27}$$

or simply

$$\frac{\partial \psi_z}{\partial y} = \frac{\partial \psi_y}{\partial z}. \tag{2.28}$$

This, however, is neither explicitly solved anywhere in the solution procedure nor does it form part of the specified boundary conditions, and it follows that there is no guarantee that Eq. (2.28) would in fact be satisfied. One may now use the same argument to raise some doubts about the correctness of the Hirasaki and Hellums approach, as it enforces only the zero through-flow condition. How can one be sure that the slip velocities would vanish (or near enough so) on the boundaries? This question may be answered by considering the following hypothetical situation:

Suppose that after a number of iterations of the solution procedure, the tangential velocity $w = \delta_x \psi_y - \delta_y \psi_x$ at a certain point on the above-mentioned stationary boundary has been incorrectly predicted by the Hirasaki and Hellums formulation (i.e., some slip exists). However, w on the boundary is never actually calculated from the vector potential. This is because the calculation of w from $\boldsymbol{\psi}$ using central differences would require a non-existing value of ψ_y outside the boundary. Further, the velocity at the boundaries should constitute part of the boundary conditions, and not part of the solution. Hence, w (like the other components of $\mathbf{V}$) is instead set to zero. Figure 2.4 shows an example of this situation. The setting of a vanishing velocity on the boundary in this case has the following effects:

(1) In the Hirasaki and Hellums formulation, $\psi_y = \psi_z = 0$ on this boundary. Hence, $u = \delta_y \psi_z - \delta_z \psi_y = 0$, so that setting the normal component u to zero is consistent with the prescribed vector potential boundary conditions.

(2) It is well known that a velocity field which is evaluated numerically from a vector potential satisfies the finite difference form of the continuity equation to

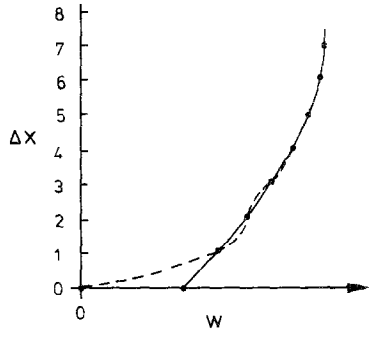

FIG. 2.4. The effect of assuming zero slip in the Hirasaki and Hellums approach. Dashed line, assumed profile; solid line, actual profile.

machine accuracy. Hence, if the velocity at a certain node is assigned to some value which differs from that produced by the vector potential, then the discretised dilatations at adjacent nodes (assuming central differencing is used) could become non-vanishing. This has the implication that the assigned boundary values of u, v, and w, if different from those represented by the vector potential, can affect the dilatation at nodes which lie on the boundary and/or are one mesh point away from it. However, it may be shown that the tangential components of velocity may be arbitrarily modified without affecting the discretised dilatation at one mesh interval from the boundary. For example, at the node $(2, j, k)$, the finite difference representation of $\nabla \cdot \mathbf{V}$ is given by

$$\nabla \cdot \mathbf{V}(2, j, k) = \frac{u(3, j, k) - u(1, j, k)}{2\,\Delta x} + \frac{v(2, j+1, k) - v(2, j-1, k)}{2\,\Delta y} + \frac{w(2, j, k+1) - w(2, j, k-1)}{2\,\Delta z}. \tag{2.29}$$

Since the only boundary value appearing in Eq. (2.29) is $u(1, j, k)$, which being the normal component is not modified, then $\nabla \cdot \mathbf{V}$ at this node must remain unaltered irrespective of what is assigned to $v(1, j, k)$ and $w(1, j, k)$. On the boundary itself, it is not possible to examine $\nabla \cdot \mathbf{V}$ explicitly and consistently as central differencing cannot be used. But it is argued that since $u(1, j, k) = 0$, any creation or destruction of mass implied by a non-zero dilatation would have to be confined to within the boundary as no mass can actually come out of, or through, such a boundary. And if further $v(1, j, k)$ and $w(1, j, k)$ are assigned to zero, creation or destruction of mass on this boundary cannot be possible. This implies that the assignment of the tangential velocity to zero on the boundary using the Hirasaki and Hellums formulation assures the satisfaction of the equation of continuity throughout the region.

(3) The discrepancy between the assigned non-slip velocity and the slip velocity inferred by the vector potential (assuming that the Hirasaki and Hellums approach initially produces some slip) forms a feedback mechanism which tends to reduce the error in subsequent iterations. This is achieved directly through the vorticity boundary conditions. In this example, the y-component of vorticity at $x = 0$ $(i = 1)$ is affected by the assumption of $w = 0$. Since on this plane

$$\zeta_y = -\frac{\partial w}{\partial x} \tag{2.30}$$

the resulting numerical value of ζ_y on the boundary in this example would be increased (see Fig. 2.4), and in turn induces an increase in shear which is necessary for diminishing the slip. A similar argument also holds when the slip is in the

negative direction. It is interesting here to point out that in the vorticity–vector potential formulation, using the Hirasaki and Hellums boundary conditions, it is vital that the vorticity boundary formulation incorporates the non-slip condition. Ozoe et al. [5] found that when the boundary vorticity was formulated in terms of the vector potential only (i.e., the direct application of Eq. (2.5)), the velocity profiles did not extrapolate smoothly to zero, whilst good results were obtained when the boundary vorticities were expressed in terms of the velocities (similar to that of Eq. (2.30)). This finding also serves to strongly support the foregoing argument.

Consider now the Richardson and Cornish formulation. From the definition of velocity and the boundary condition of ψ as given by Eq. (2.26), the tangential velocity components, v and w, are necessarily zero on the boundaries. But as mentioned earlier, the normal velocity component, u, as calculated from the vector potential may be non-zero, implying that fluid may be crossing the boundaries. Setting the normal velocity component to zero does nothing to alleviate the problem. From Eq. (2.29), it is seen that an alteration of $u(1, j, k)$ leads to a non-zero dilatation at nodes one mesh from the boundary. That is, the correction of u at $i = 1$ merely shifts the "leakage" to $i = 2$. This problem was encountered in the work of Leonardi et al. [9]. There also seems to be no natural mechanism by which the iteration process can effectively rectify this problem. The term which can bring about any feedback in this case in $\partial u/\partial x$ at $i = 1$ or $i = 2$. Since this term does not appear in any of the vorticity boundary conditions, and appears only as one of the many terms in the vorticity transport equation, little (if any) effort can be made to stop the "leaks." As a consequence, non-convergence or convergence to erroneous solutions can be expected. In an attempt to counter this lack of natural feedback, Reizes et al. [12] actually calculated the "leakage" velocities from the vector poten-

introduction of an extra variable (the scalar potential), the vector–scalar potential formulation also produced unsatisfactory results. It has later been shown by Wong and Reizes [8] that the inclusion of the scalar potential in a non-staggered grid system can lead to substantial errors, and should be avoided if possible.

3. A New Approach

Although the Hirasaki and Hellums formulation for simply connected regions has the necessary properties which would permit a stable and meaningful convergence, it was shown earlier that difficulties may arise in multiply connected regions. In this section, a new approach is developed to handle the boundary conditions of the vector potential for multiply connected regions of simple, but nevertheless important, geometries—i.e., regions whose boundaries coincide with the coordinate surfaces. Extension of the technique to more complex regions may also be possible by applying a suitable transformation procedure.

Consider the doubly connected region confined by the concentric cylinders as shown in Fig. 3.1. The application of the Hirasaki and Hellums formulation results in the set of vector potential boundary conditions

$$\psi_r = \psi_\theta = \frac{\partial \psi_z}{\partial z} = 0 \tag{3.1a}$$

on the top and bottom plates,

$$\frac{\partial (r\psi_r)}{\partial r} = \psi_\theta = \psi_z = 0 \tag{3.1b}$$

at $r = r_i$, and

$$\frac{\partial (r\psi_r)}{\partial r} = \psi_\theta = 0, \qquad \psi_z = K \tag{3.1c}$$

at $r = r_o$. (See Fig. 3.1.)

As for the rectangular annulus considered in Section 2, the analysis again resulted in one unknown. In this case, ψ_z on the outer cylinder has yet to be determined. To this end, we make use of the condition of no-slip on this surface, which requires that

$$v = \frac{\partial \psi_r}{\partial z} - \frac{\partial \psi_z}{\partial r} = 0, \tag{3.2}$$

or

$$\frac{\partial \psi_z}{\partial r} = \frac{\partial \psi_r}{\partial z}, \tag{3.3}$$

where v is the component of velocity in the circumferential direction.

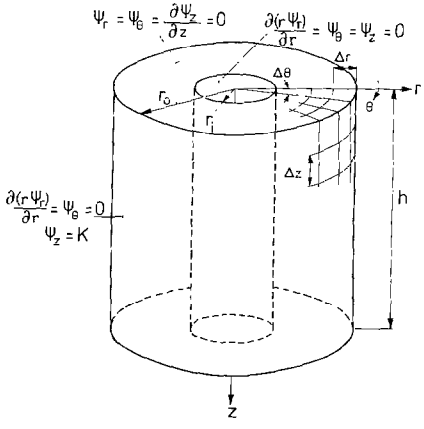

FIG. 3.1. Solution region and the boundary conditions for ψ in the centrifuge example.

Equation 3.3 appears as a usable form of boundary condition for ψ_z, as $\partial\psi_r/\partial z$ can readily be calculated from the latest solution of ψ_r. However, the direct use of Eq. (3.3) (i.e., using it as a Neumann condition) would lead to problems similar to those encountered by the Richardson and Cornish formulation. To ensure no leakage, the fact that ψ_z equals a constant on this surface must be incorporated.

Let there be L, M, and N mesh intervals in the $r(i)$, $\theta(j)$, and $z(k)$ directions, respectively. The second-order finite difference form of Eq. (3.3) at (L, j, k) may be rearranged to give

$$\psi_z(L, j, k) = \frac{1}{3}\left\{\frac{\Delta r}{\Delta z}\left[\psi_r(L, j, k+1) - \psi_r(L, j, k-1)\right] + 4\psi_z(L-1, j, k) - \psi_z(L-2, j, k)\right\}, \tag{3.4}$$

so that ψ_z may be evaluated at each point on the outer cylinder. Due to the truncation errors involved in the differencing of Eq. (3.3) and the lag between the solutions of ψ_r and ψ_z (assuming that the solution has not yet converged), $\psi_z(L, j, k)$ as evaluated from Eq. (3.4) would not be expected to be constant over the whole of the outer cylinder. It is, however, likely that the errors in predicting $\psi_z(L, j, k)$ from Eq. (3.4) for all the points over this boundary are scattered around zero, so that their average would be a good estimate of the required constant. (Note that even if the mean error is not zero, it is, at worst, of the same order as the individual truncation errors.) Hence, the boundary value of ψ_z at the surface $r = r_o$ is proposed to be

$$\psi_z(L, j, k) = \frac{1}{3M(N-2)}\sum_{j=1}^{m}\sum_{k=2}^{N-1}\left\{\frac{\Delta r}{\Delta z}\left[\psi_r(L, j, k+1) - \psi_r(L, j, k-1)\right] + 4\psi_z(L-1, j, k) - \psi_z(L-2, j, k)\right\}. \tag{3.5}$$

From the latest solution of ψ_r and ψ_z, the boundary value $\psi_z(L, j, k)$ may be evaluated by Eq. (3.5) and updated after each iteration.

To test the proposed scheme, two special cases of multiply connected flows were considered, in which other solution methods are available. The first was the solution to the incompressible flow within a concentric annular cavity with a rotating inner cylinder. (See Fig. 3.1.) Since this was an axisymmetric problem, it degenerated into a quasi two-dimensional problem which may be solved by any of the well-established 2-D techniques (e.g., [11]). The radius ratio r_o/r_i and aspect ratio $h/(r_o - r_i)$ were 2 and 1, respectively. Because of the axisymmetry, it was sufficient to allocate only four mesh planes in the circumferential direction. Each of these mesh planes incorporated a uniform grid system of 21×21. To cope with this relatively coarse mesh, the Reynolds number (based on the gap dimension) was restricted to only 100. Figure 3.2 shows the comparison of results obtained by the proposed method and the axisymmetric solution obtained by the stream function/vorticity/swirl-velocity formulation of [11]. As may be seen, the agreement

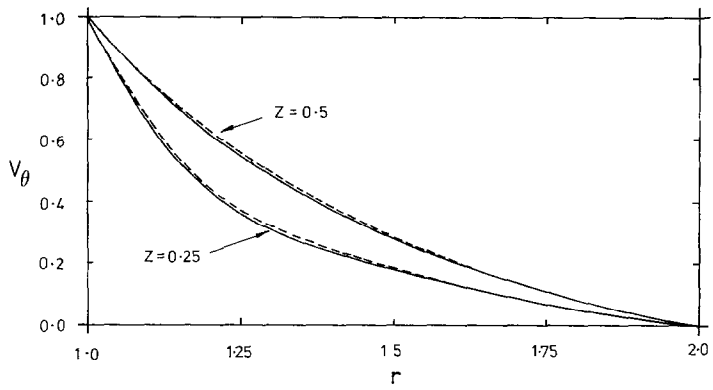

FIG. 3.2. Comparison of circumferential velocities in the centrifuge example. Solid line, present analysis; dashed line, axisymmetric solution.

was excellent, indicating that the proposed method was able to accurately predict the circumferential flow rate and therefore the required constant.

The second test was a natural convection problem between two coaxial horizontal square prisms with the inner walls uniformly heated. The fluid used was compressible air whose density was assumed to be a function of temperature only. The outer box, with a length-to-width ratio of two, was fitted with a uniform grid of $25 \times 25 \times 25$, with the inner prism occupying the central $5 \times 5 \times 25$ points. A Rayleigh number, Ra (based on the width of the outer box), of 50,000 was considered. In addition to the equations of motion presented in Section 2, the energy transport equation and an equation of state were included in the solution procedure. Because of the symmetry, the net circumferential flow rate in this case must necessarily be zero. It therefore implies that ψ_z on the surface of both cylinders must be identical. In the test problem, ψ_z on the outer walls was set to zero, whilst on the inner walls, $\psi_z = K$ was predicted by the proposed method. It was found that, irrespective of what was initially assigned to K, the converged value (computed in single precision on a VAX 11/780) was of the order of 10^{-8} compared to a maximum value of the solution of 4.38. Figure 3.3 shows a stream-line

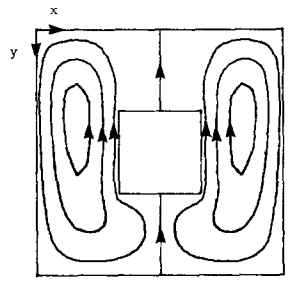

FIG. 3.3. Stream-lines on the mid $x - y$ plane of the symmetrical natural convection example.

plot at the central $x-y$ plane which clearly illustrates the symmetry of flow and the absence of any net flow around the annulus. The validity of the solution was further verified by solving the same problem in only one-half of the solution region ($0 \leqslant x \leqslant 0.5$). Since the solution region was then considered simply connected, the Hirasaki and Hellums formulation was usable, which produced results which were, for all practical purposes, identical to those obtained by the proposed method.

4. Other Results and Discussion

Due to the lack of three-dimensional multiply connected flow studies in the literature, comparison of the proposed technique with other models was not possible. Instead, a model problem was proposed, which perhaps can be used as a benchmark for future comparison purposes. The problem as illustrated in Fig. 4.1 was chosen for this purpose because of its geometric simplicity, true three-dimensionality, and, of course, multiple connectivity, as well as for having some resemblance to real problems and the possibility of interesting features such as flow separations and corner effects. It was essentially a natural convection problem in a region confined between two coaxial horizontal prisms of square cross sections. The inner surfaces were heated whilst one of the outer vertical side walls and both of the end plates were insulated. The remaining surfaces were cold. The temperatures of the hot and cold surfaces were 288K and 300K, respectively, and Rayleigh numbers of 5000 and 50,000 were studied. The fluid was air, with variable density (assumed to be a function of temperature only), but constant conductivity and viscosity. A uniform mesh of $31 \times 31 \times 31$ for the outer prism was used, with the inner prism occupying the central $11 \times 11 \times 31$ points.

Unlike the symmetric problem of Section 3, the proposed scheme yielded non-zero values of ψ_z on the inner surfaces, indicating that there were net "circumferen-

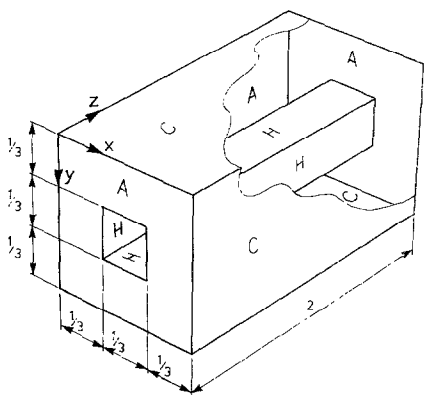

FIG. 4.1. Schematic diagram of asymmetrical natural convection problem. A = Adiabatic; C = cold; H = hot.

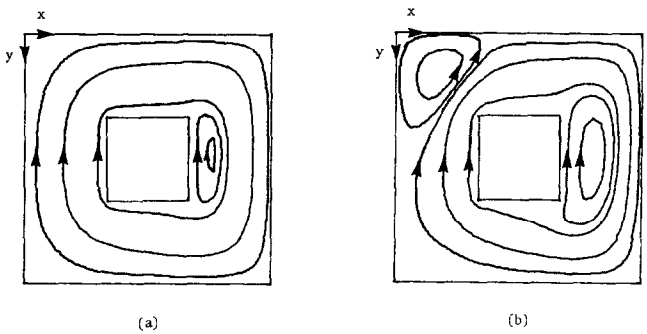

(a) (b)

FIG. 4.2. Stream-lines on the mid $x-y$ plane for the asymmetric convection problem. (a) Ra = 5000, (b) Ra = 50,000.

tial" flows around the square annuli. In the cases considered, the inner boundary values of ψ_z were 1.114 and 4.356 for Ra = 5000 and 50,000, respectively. The resulting net flow movement is clearly visible in Fig. 4.2, where the stream-lines on the central $x-y$ plane are shown. This clockwise motion of the main stream was the result of the higher average temperatures on the side nearer the adiabetic wall (see Fig. 4.3). Smaller clockwise circulations were also present on the side nearer the cold wall as a result of the differential heating between the hot inner walls and the vertical cold wall of the outer box. The extent of this separation was seen to increase with increases in Ra. The higher Ra results also indicated substantial flow separations at the upper corner of the adiabatic wall as a result of the higher velocities.

The fluid motions at other cross sections were much more complex as the stream-lines were described generally in three dimensions. To obtain these stream-lines, the technique of particle tracking, similar to that used by Mallinson and de Vahl Davis [4], was employed. Particles were released at various locations with the resulting tracks as shown in Figs. 4.4 to 4.7. For the lower Ra case, the flow field

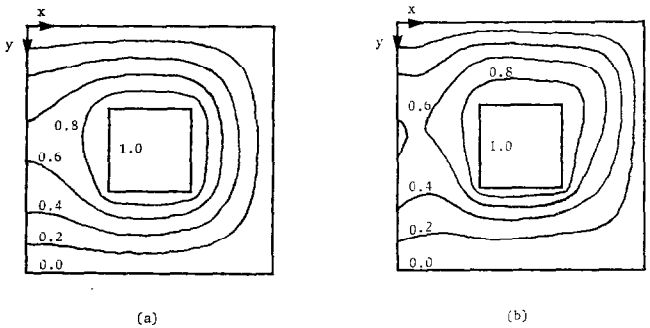

(a) (b)

FIG. 4.3. Temperature contours on the mid $x-y$ plane for the asymmetric convection problem. (a) Ra = 5000, (b) Ra = 50,000.

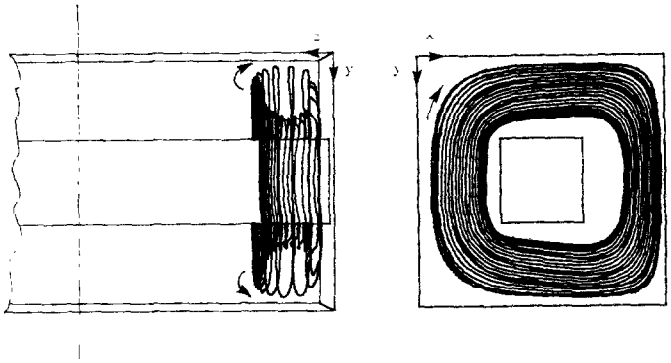

FIG. 4.4. Particle released at (0.2, 0.2, 0.05), Ra = 5000.

may be divided roughly into three main regimes, which were typified by the particle tracks presented. Regime 1 consisted of tracks which spiraled back and forth on a nest of toroidal surfaces situated closed to the end plates ($0 \lesssim z \lesssim 0.33$, $1.67 \lesssim z \lesssim 2$). The particles moved away from the ends near the inner side, and returned along the outer side of the toroids (see Fig. 4.4). A second set of spirals (regime 2) was apparent between the heated inner walls and the cold vertical side of the outer box. Figure 4.5 shows a particle released at (0.70, 0.50, 0.01), which followed a tightly coiled path between the inner walls and the toroidal zone, moving away from the ends whilst increasing in size. When a sufficient size was reached, this path began to coil around the rod and eventually followed a track which encased the toroidal zone, back to its starting point. For clarity, the latter part of this tightly coiled path is not shown in Fig. 4.5. In the central region (regime 3, which accounts for approximately 60% of the solution region), the tracks reduced to simple rings which were essentially two-dimensional and resembled those shown in Fig. 4.2a.

As the Rayleigh number was increased, the toroidal region merged into an expanding regime 2 to form a series of paths similar to that shown in Fig. 4.6. The

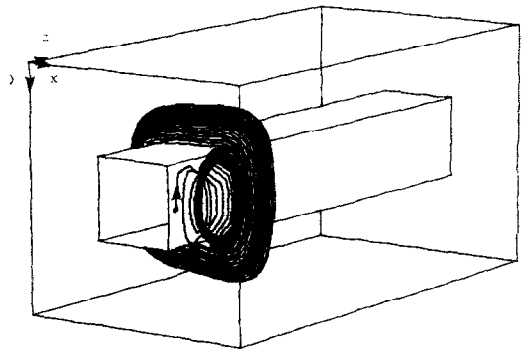

FIG. 4.5. Particle released at (0.7, 0.5, 0.01), Ra = 5000.

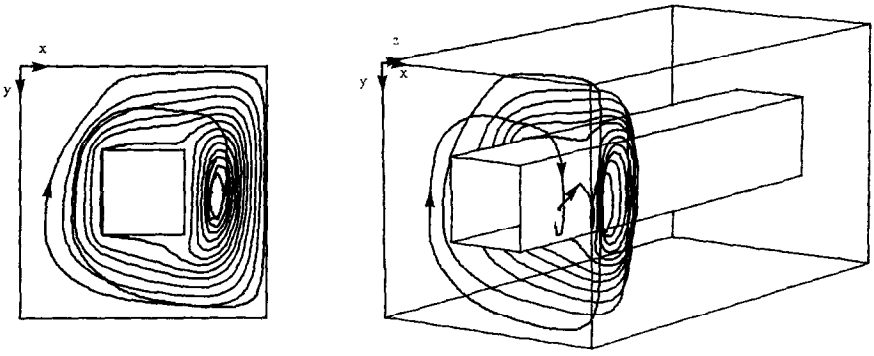

FIG. 4.6. Particle released at (0.77, 0.5, 0.1), Ra = 50,000.

dilation of regime 2 also caused regime 3 to be pushed further towards the central region. The increase in the circumferential velocity due to the increase in Ra also tended to encourage flow separations at the corners. In Fig. 4.7, it is seen that for Ra = 50,000, a fourth regime was created due to the flow separation in the upper corner of the adiabetic wall.

Tests were also conducted to determine the influence of the initial estimate of the unknown boundary value of ψ_z on the solution. To keep the amount of computation to a reasonable level, Ra and the number of mesh points were reduced to 100 and $13 \times 13 \times 13$, respectively. With all other fields initially set to zero, it was found that a unique solution was obtained irrespective of the initial estimate used (provided that the solution procedure did not diverge). As to be expected, however, the number of iterations required to reach convergence depended on how good the initial estimate was. In order to approach the correct value as quickly as possible, two methods were tested and found to be useful.

The first involved the application of an overrelaxation factor to Eq. (3.5) such

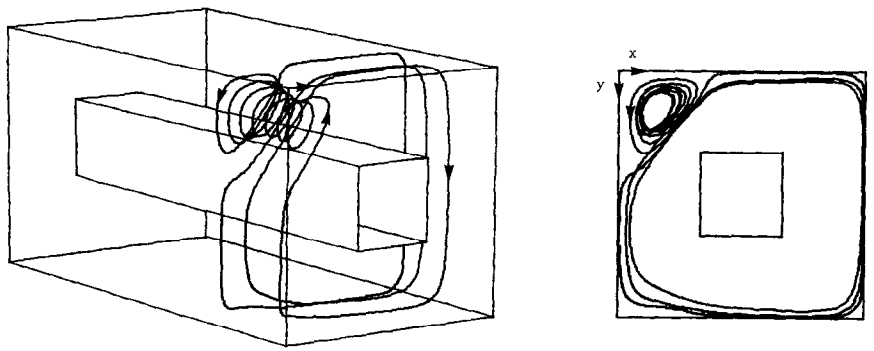

FIG. 4.7. Particle released at (0.1, 0.1, 0.1), Ra = 50,000.

TABLE 4.1

Effects of Initial Estimate of K and Relaxation Factor in Eq. (4.1) on the Convergence Rate

Initial estimate of K	2.571×10^{-3}	2.571×10^{-2}	2.571	0	0	0	0	0	2.571×10^{-2}	Exponential extrapolation
Relaxation factor, λ	1	1	1	1	2	3	4	5	0	
Number of iterations to convergence	160	149	233	162	102	83	148	Diverged	56	85
Value of K at convergence	2.571×10^{-2}									

that at the mth iteration, the new estimate of the unknown vector potential $\psi_z = K^m$ was given by

$$K^m = K^{m-1} + \lambda(K' - K^{m-1}), \tag{4.1}$$

where K' is obtained from Eq. (3.5) and λ is a suitable weighting factor.

In general, setting λ just above 1 should accelerate the rate of convergence. In the test problem, convergence was obtained with λ set to as high as 4. The optimum value appeared to be near 3, which corresponded to a reduction in computing time of about 50%. The results for other values of λ are as shown in Table 4.1.

Another method tested was a more elaborate extrapolation procedure, in which the trend of the increase or decrease of K' was used to predict the asymptotic limit. For this test problem, an exponential curve was fitted through three successive values of K' after every m ($\geqslant 3$) iterations. K was then extrapolated to infinity or to n steps, depending on whether the trend was exponentially decaying or increasing. It was found that $m = 6$ and $n = 3$ produced substantial improvements, which reduced the number of iterations required from 162 (no extrapolation used) to 85.

It should be pointed out that the above techniques for speeding up the process of searching for the correct value of K are by no means exhaustive, and the reader is invited to explore other possibilities. Judging from the fact that if K were fixed at the converged value throughout the iterative procedure only 56 iterations were required, there is probably still room for further improvement. However, it is expected that some price must be paid for not having the prior knowledge of K.

Concluding Remarks

A new approach has been devised to permit the vector potential to be used in an important class of multiply connected regions. Its successful application was

demonstrated by the solution of several free and forced convection problems in annular cavities. The scheme was found to be stable, and suggestions were made for increasing its rate of convergence.

ACKNOWLEDGMENT

The authors wish to thank Dr. E. Leonardi for implementing the proposed formulation to the centrifuge program as well as for providing the axisymmetric results presented in Section 3.

REFERENCES

1. K. AZIZ AND J. D. HELLUMS, *Phys. Fluids* **10** (1967), 314.
2. G. J. HIRASAKI AND J. D. HELLUMS, *Quart. Appl. Math.* **26** (1968), 331.
3. S. M. RICHARDSON AND A. R. H. CORNISH, *J. Fluid Mech.* **82** (1977), 309.
4. G. D. MALLINSON AND G. DE VAHL DAVIS, *J. Comput. Phys.* **12** (1973), 435.
5. H. OZOE, K. YAMAMOTO, S. W. CHURCHILL, AND H. SAYAMA, *J. Heat Transfer* **98** (1976), 202.
6. Y. A. S. AREGBESOLA AND D. M. BURLEY, *J. Comput. Phys.* **24** (1977), 398.
7. G. J. HIRASAKI AND J. D. HELLUMS, *Quart. Appl. Math.* **28** (1970), 293.
8. A. K. WONG AND J. A. REIZES, *J. Comput. Phys.* **55** (1984), 98.
9. E. LEONARDI, J. A. REIZES, AND G. DE VAHL DAVIS, *in* "2nd International Conference on Numerical Methods in Laminar and Turbulent Flows" (C. Taylor and B. A. Schrefler, Eds.), p. 995, Pineridge Press, Swansea, Wales, 1981.
10. P. J. ROACHE, "Computational Fluid Dynamics," Hermosa Publishers, Albuquerque, N.M., 1972.
11. E. LEONARDI, J. A. REIZES, AND G. DE VAHL DAVIS, *in* "Heat Transfer 1982" (U. Grigall, E. Hahner, K. Stephan, and J. Straub, Eds.), p. 69, Hemisphere Pub. Corp., 1982.
12. J. A. REIZES, E. LEONARDI, AND G. DE VAHL DAVIS, *in* "Computational Techniques and Applications" (J. Noye and C. Fletcher, Eds.), p. 903, North-Holland, Amsterdam, 1984.